

# Global Land Cover Classification Based on Microwave Polarization and Gradient Ratio (MPGR)

Mukesh Boori and Ralph Ferraro

**Abstract** Microwave polarization and gradient ratio (MPGR) is an effective indicator for characterizing the land surface from sensors like EOS Advanced Microwave Scanning Radiometer (AMSR-E). Satellite-generated brightness temperatures (BT) are largely influenced by soil moisture and vegetation cover. The MPGR combines the microwave gradient ratio with polarization ratio to determine surface characteristics (i.e., bare soil/developed, ice, and water) and under cloud covered conditions when this information cannot be obtained using optical remote sensing data. This investigation uses the HDF Explorer, Matlab, and ArcGIS software to process the pixel latitude, longitude, and BT information from the AMSR-E imagery. This paper uses the polarization and gradient ratio from AMSR-E BT for 6.9, 10.7, 18.7, 23.8, 36.5, and 89.0 GHz to identify seventeen land cover types. A smaller MPGR indicates dense vegetation, with the MPGR increasing progressively for mixed vegetation, degraded vegetation, bare soil/developed, and ice and water. This information can help improve the characterization of land surface phenology for use in weather forecasting applications, even during cloudy and precipitation conditions which often interferes with other sensors.

**Keywords** AMSR-E • MODIS • MPGR • Microwave remote sensing • GIS • Climate change • CHAPTER

---

M. Boori (✉)

National Research Council (NRC), College Park, USA  
e-mail: msboori@gmail.com

M. Boori · R. Ferraro

NOAA/NESDIS/STAR/Satellite Climate Studies Branch and Cooperative Institute for Climate and Satellites (CICS), ESSIC, University of Maryland, College Park, MD, USA  
e-mail: ralph.r.ferraro@noaa.gov

# 1 Introduction

Timely monitoring of natural disasters is important for minimizing economic losses caused by floods, drought, etc. Access to large-scale regional land surface information is critical to emergency management during natural disasters. Remote sensing of land cover classification and surface temperature has become an important research subject globally. Many methodologies use optical remote sensing data (e.g. Moderate Resolution Imaging Spectro Radiometer—MODIS) and thermal infrared satellite data to retrieve land cover classification and surface temperature. However, optical and thermal remote sensing data is greatly influenced by cloud cover, atmospheric water content, and precipitation, making it difficult to combine with microwave remote sensing data [1]. Thus, optical or thermal remote sensing data cannot be used to retrieve surface temperature during active weather conditions. However, microwave remote sensing can overcome these disadvantages. Passive microwave emission penetrates non-precipitating clouds, providing a better representation of land surface conditions under nearly all weather conditions. Global data are available daily from microwave radiometers, whereas optical sensors (e.g., Landsat TM, ASTER, and MODIS) are typically available globally only as weekly products due to clouds. The coarse spatial resolution of passive microwave sensors is not a problem for large scale studies of recent climate change [2]. For example McFarland et al. [3] showed that surface temperature for crop/range, moist soils, and dry soils can be retrieved using linear regression models from the Special Sensor Microwave/Imager (SSM/I) BT.

Microwave polarization ratio (PR; the difference between of the first two stokes parameters (H- and V-polarization) divided by their sum) and gradient ratio (GR; the difference of two Stokes Parameters either H or V with different frequency divided by their sum) correspond with seasonal changes in vegetation water content and leaf area index [4–6]. The possibility of simultaneously retrieving “effective surface temperature” with two additional parameters, vegetation characteristics and soil moisture, has been demonstrated, mainly using simulated datasets [7–9]. The MPGR is sensitive to the NDVI [4, 10], as well as open water, soil moisture, and surface roughness [11]. Paloscia and Pampaloni [12] used microwave radiometer to monitor vegetation and demonstrate that the MPGR is very sensitive to vegetation types (especially for water content in vegetation), and that microwave polarization index increases exponential with increasing water stress index. The polarization index also increases with vegetation growth [13]. Since microwave instruments can obtain accurate surface measurements in conditions where other measurements are less effective, MPGR has great potential for observing soil moisture, biological inversion, ground temperature, water content in vegetation, and other surface parameters [1]. This paper derives MPGR and uses it to discriminate different land surface cover types, which is turn will help improve monitoring of weather, climate, and natural disasters.

**Table 1** MODIS land cover classes with their code

0 Water	09 Savannas
1 Evergreen needle leaf forest	10 Grasslands
2 Evergreen broad leaf forest	11 Permanent wetlands
3 Deciduous need leaf forest	12 Croplands
4 Deciduous broad leaf forest	13 Urban built-up
5 Mixed forest	14 Cropland natural vegetation mosaic
6 Closed shrub lands	15 Snow Ice
7 Open shrub lands	16 Barren Sparsely Vegetated
8 Woody savannas	

## 2 Data Used

The Advanced Microwave Scanning Radiometer (AMSR-E) was deployed on the NASA Earth Observing System (EOS) polar-orbiting Aqua satellite platform. The AMSR-E sensor measures vertically (V) and horizontally (H) polarized BT at six frequencies (6.9, 10.7, 18.7, 23.8, 36.5, and 89.0 GHz) at a constant Earth incidence angle of  $55^\circ$  from nadir. In this study, we use AMSR-E level 2A product (AE\_L2A), and the daily 25 km resolution global Equal Area Scalable Earth (EASE) Grid BT provided by the National Snow and Ice Data Center (NSIDC). AMSR-E is a successor to the Scanning Multi-channel Microwave Radiometer (SMMR) and SSM/I instruments, first launched in 1978 and 1987, respectively. AMSR-E provides global passive microwave measurements of terrestrial, oceanic, and atmospheric variables for investigation of the global water and energy cycles. MODIS land cover data (MCD12Q1) was acquired from the NSIDC and used to determine land cover information. The MODIS land cover type product contains classification schemes, which describe land cover properties derived from observations spanning a year's input of Terra data. The primary land cover scheme identifies 17 land cover classes defined by the international Geosphere Biosphere Programme (IGBP), including 11 natural vegetation classes, 3 developed and mosaicked land classes, and 3 non-vegetation classes (Table 1).

## 3 Methodology

The derivation of microwave polarization ratio (PR) and gradient ratio (GR) is based on the radiance transfer theory as follows:

$$B_f(T) = 2hf^3/c^2 \left( e^{hf/kT} - 1 \right) \quad (1)$$

$$B_f(T) = 2kT/\lambda^2 [1/1 + (hf/kT) + (hf/kT)^2 + \dots + (hf/kT)^n] \quad (2)$$

Planck's function (Eq. 1) describes the relationship between spectral radiance emitted by a black body and real temperature, where  $T$  is the temperature in Kelvin,  $B_f(T)$  is the spectral radiance of the blackbody at  $T$  Kelvin,  $h$  is the Planck constant,  $f$  is the frequency of the wave band,  $c$  is the light speed, and  $k$  is Boltzman constant. On the basis of the Taylor series expansion equation, Planck's function can be written as Eq. 2.

$$B_f(T) = 2kT/\lambda^2 \quad (3)$$

$$T_f = \tau_f \varepsilon_f T_{soil} + (1 - \tau_f)(1 - \varepsilon_f) \tau_f T_a^\downarrow + (1 - \tau_i) T_a^\uparrow \quad (4)$$

In most passive microwave applications, the value of the term  $hf/kT$  can be assumed to be zero. Hence Planck's function can be simplified as Eq. (3). For land cover surface temperature ground emissivity and atmospheric effects are considered in the general radiance transfer equations for passive microwave remote sensing [14, 15] so Eq. 3 can be rewrite as Eq. (4), where  $T_f$  is the BT in frequency  $f$ ,  $T_{soil}$  is the average soil temperature,  $T_a$  is the average atmosphere temperature,  $B_f(T_{soil})$  is the ground radiance,  $B_f(T_a^\downarrow)$  and  $B_f(T_a^\uparrow)$  are the down-welling and up-welling path radiance, respectively,  $\tau_f(\theta)$  is the atmosphere transmittance in frequency  $f$  at viewing direction  $\theta$  (zenith angle from nadir), and  $\varepsilon_f$  is the ground emissivity. From Eq. (4), a linear relationship is evident between remotely sensed BT and land surface temperature.

Furthermore, we assume that a vegetation layer can be considered a plane, parallel, absorbing, and scattering medium at a constant temperature  $T_c$  upon the soil surface. The brightness temperature  $T_p(\tau, \mu)$  of the radiation emitted by vegetation canopy at an angle  $\theta$  from the zenith can be written as follows [13]:

$$T_p(\tau, \mu) = (1 - w) \left( 1 - e^{-\tau/\mu} \right) T_c + \varepsilon_p T_{soil} e^{-\tau/\mu} \quad (5)$$

where  $p$  stands for horizontal ( $H$ ) or vertical ( $V$ ) polarization,  $\mu = \cos\theta$ .  $\tau$  is the equivalent optical depth,  $w$  is the single scattering albedo. The two parameters (background and atmospheric effect) can characterize the absorbing and scattering properties of vegetation, respectively.  $\varepsilon_p$  is the soil emissivity for the  $p$  polarization.

MPGR Eq. (6a) and (6b) is an effective indicator for characterizing the land surface vegetation cover density. The polarization ratio used in the study can be described as Eq. (6a)

$$PR(f) = [BT(fV) - BT(fH)] / [BT(fV) + BT(fH)] \quad (6a)$$

And the gradient ratio as Eq. (6b)

$$[GR(f1p_f2p) = BT(f1p) - BT(f2p)] / [BT(f1p) + BT(f2p)] \quad (6b)$$

where BT is the brightness temperature at frequency  $f$  for the polarized component  $p$ . When there is little vegetation cover over the land surface, the value of  $\tau$  can be defined as zero. So the MPGR of bare ground can be written as Eq. (7a) for polarization and Eq. (7b) for gradient ratio.

$$\text{PR}(f) = [\varepsilon(fV) - \varepsilon(fH)] / [\varepsilon(fV) + \varepsilon(fH)] \quad (7a)$$

$$[\text{GR}(f_1p_2p) = \varepsilon(f_1p) - \varepsilon(f_2p)] / [\varepsilon(f_1p) + \varepsilon(f_2p)] \quad (7b)$$

According to Paloscia and Pampaloni [13], we can assume  $\varepsilon_{\text{soil}}(\varepsilon_V + \varepsilon_H)/2$ , and  $T_c = T_{\text{soil}}$ . Then Eq. (7a, 7b) can be further simplified as

$$\text{MPGR}(\tau, \mu) \approx \text{MPGR}(0, \mu)e^{-\tau/\mu} \quad (8)$$

Since microwave radiation is polarized, it can be used to depict the condition of vegetation if the vegetation-soil is made a pattern. Equation (8) shows that MPGR mainly depends on  $\mu$  and  $\tau$ , and MPGR values fall as vegetation becomes thicker. Therefore, MPGR indicates the density of land surface vegetation cover. Vegetation cover also greatly influences the land surface temperature. Thus, we classify the land surface vegetation cover conditions into several types based on values of MPGR (Fig. 1).

## 4 Result and Discussion

To identify the behavior of each land cover class, we first selected/determined sample sites in all 17 land cover classes through the use of the ArcGIS system. Then their maximum, minimum, mean, and standard deviation were derived all horizontal and vertical AMSR-E frequencies to determine which combination of MPGR are best suited for land cover classification. We find (Fig. 2) that vertical and higher frequency are closer to actual physical land surface condition/type compared with horizontal and lower frequency. Low frequencies of AMSR-E are hardly influenced by atmospheric effects during bad weather, but they are affected by surrounding (near features) and background surface effects since they absorb less and scatter more by soil. Frequencies of 89 GHz and above are more likely to be influenced by the atmosphere than other AMSR-E bands, especially during bad weather conditions [16, 17]. Our approach makes use of the 89 GHz channels, because the 89 GHz data are influenced less by surface effects than the lower frequencies, and the 89 GHz channels have successfully been used in water and sea ice concentration retrievals under clear atmospheric conditions [18]. Lower frequencies help to distinguish the land surfaces' vegetation cover conditions. However, the BT differences between

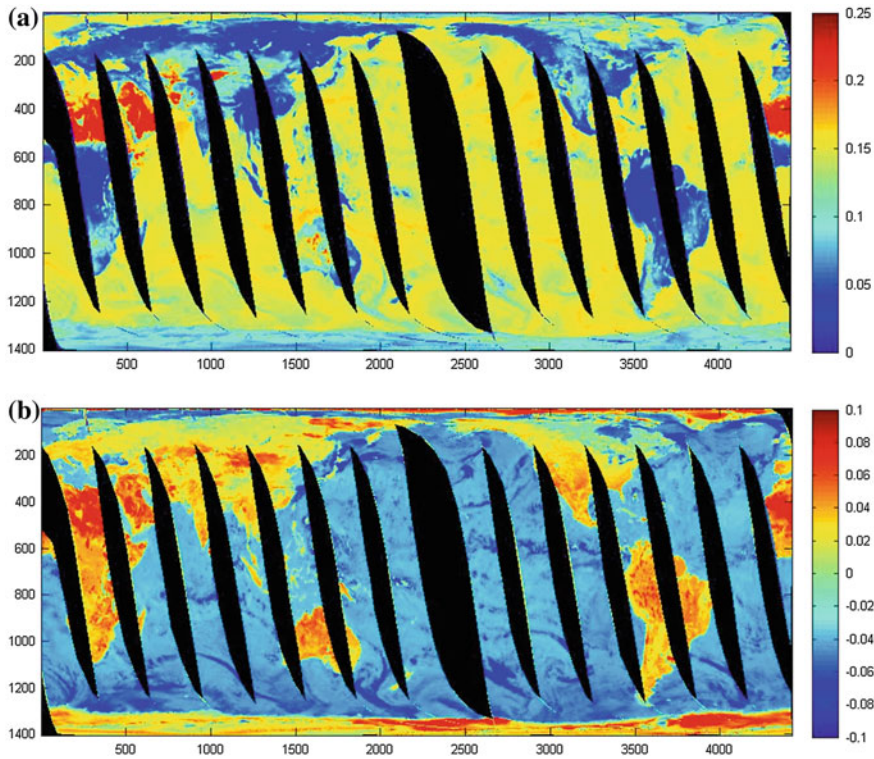


**Fig. 1** AMSR-E image with MPGR value range for **a** polarization ratio (PR 36.5) and **b** gradient ratio GR-V (36.5–18.7). In panel *a*, the dark red areas indicate deserts, dark blue represents dense vegetation, and the color in between correspond to mixed vegetation. In panel *b*, dark red highlights desert regions, and light red showing vegetation condition, yellow and sky blue showing mixed vegetation (30/09/2011). Both images clearly differentiate land and water on earth after polarization or gradient ratio

high frequencies also can be used to evaluate the influence of soil moisture and barren sparsely vegetation/bare soil.

In Fig. 2 evergreen needle leaf and broad leaf forest have higher temperatures than deciduous forest, but both forest types have lower temperatures than shrub land and savanna. Mixed forest has a much smaller range of standard deviations and always falls between evergreen and deciduous forest (Fig. 2). Close shrub has lower temperature and a smaller standard deviation than open shrub. Wetland has lower temperature than grassland and cropland due to water content. Built-up area has higher standard deviation than other land cover classes except for water and ice (Fig. 2). But in Fig. 2 it is hard to find a clear set of parameters that can uniquely identify all of the 17 land surface type. Thus, we utilize MPGR which combines much of the information and may potentially separate the 17 land surface type.

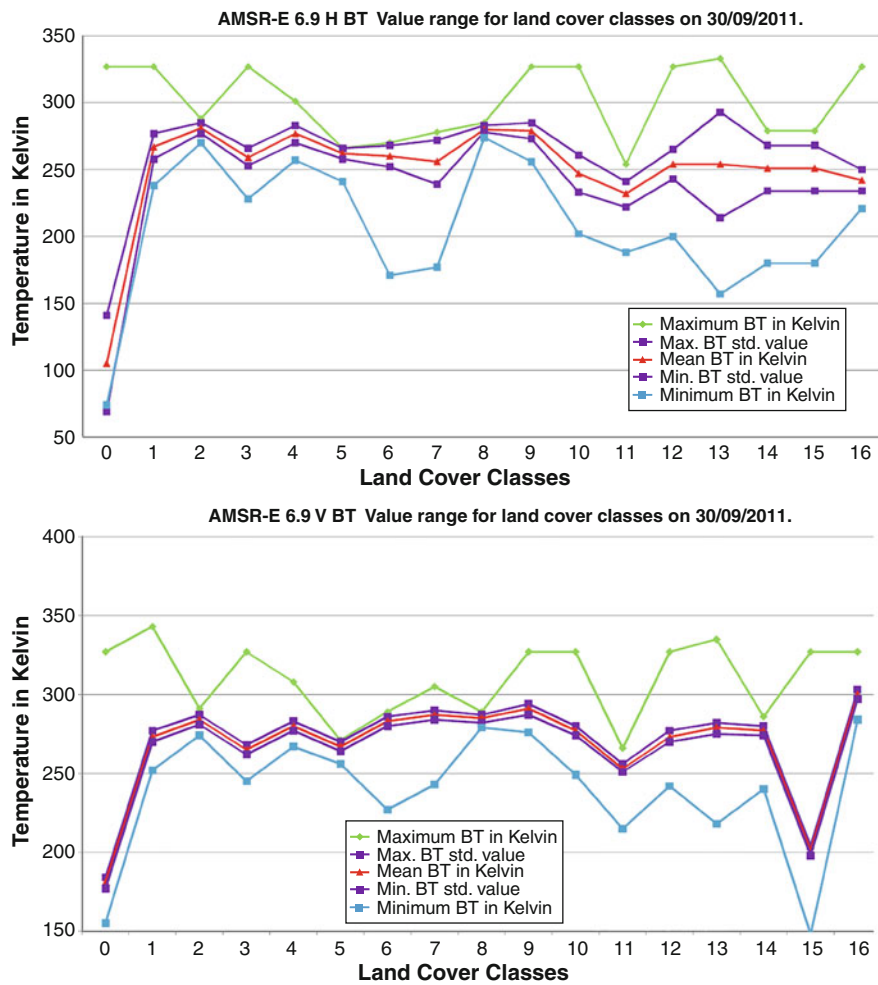


Fig. 2 Seventeen land cover classes maximum, minimum, mean and standard deviation temperature in kelvin for 6.9, 10.7, 18.7, 23.8, 36.5 and 89.0 Ghz AMSR-E frequency

Using AMSR-E frequencies and MPGR is an effective way to derive surface type based on the land surface vegetation cover classification. We used two lower frequencies (10, 18 GHz), and two higher frequencies (36, 89 GHz) for further analysis. For land cover classification on the basis of MPGR, we focused on three combinations of PR-PR, PR-GR and GR-GR, and plot two graphs for each combination (Fig. 3). The scatterplots identify all 17 land cover classes (as shown in Fig. 3). Water pixels are located at highest value in the graph, then ice, bare soil, built-up area, and grasslands, savanna, mixed vegetation, degraded vegetation and dense/evergreen vegetation, respectively.



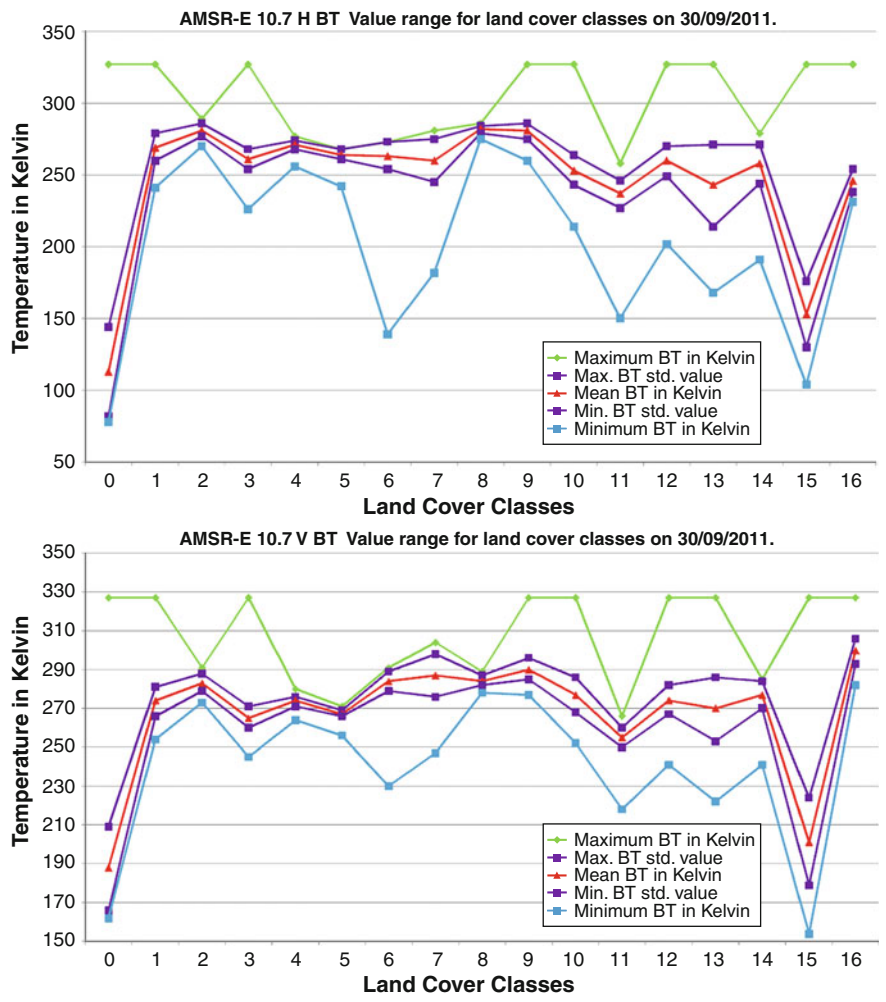


Fig. 2 continued

Table 2 shows all 17 land cover classes based on the MPGR graphs. For the PR-PR (36-18, 10-89 GHz) combination, vegetation is present from 0.0 to 0.06, and then barren/sparse vegetation or bare soil from 0.06 to 0.09, with ice between 0.09 and 0.012 and then water. For the PR-GR [18-(18-89), 10-(10-18)] combination, vegetation is from 0.0 to 0.04, bare soil from 0.06 to 0.08, and ice 0.09 to 0.12 followed by water. For the GR-GR (89-18, 36-10) combination, dense vegetation is present between -0.03 and 0.0, then normal vegetation, bare soil between 0.04 and 0.05, then snow/ice from 0.05 to 0.06, and again followed by water.



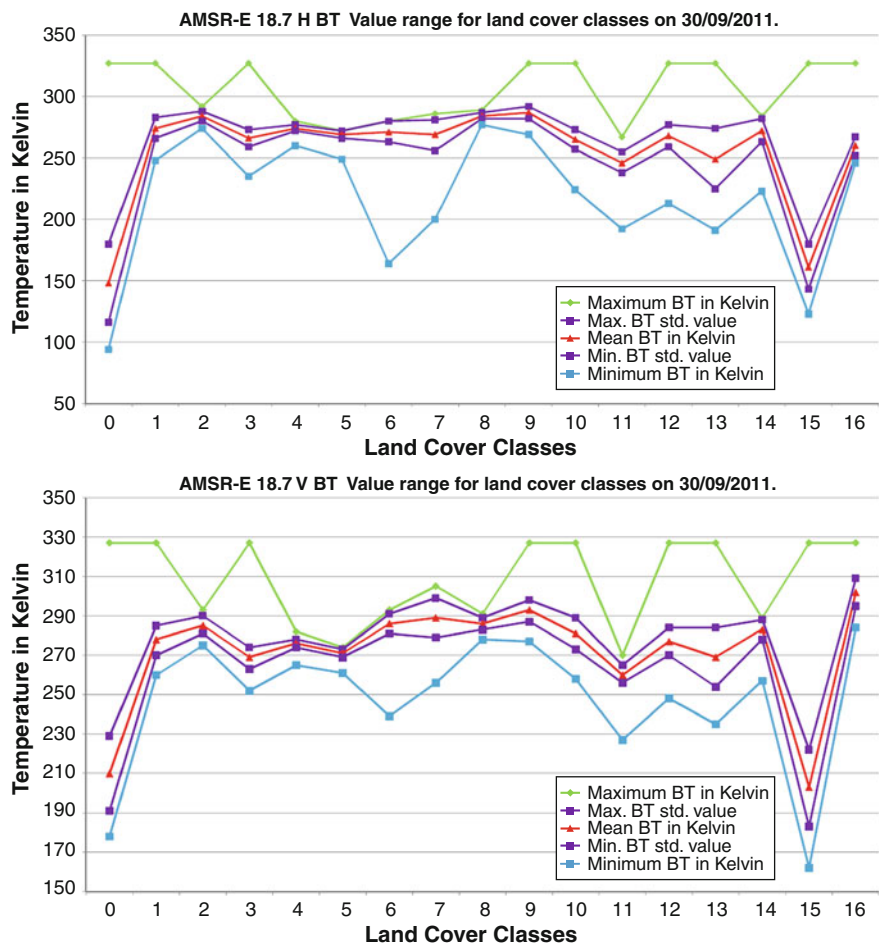


Fig. 2 continued

Table 3 and Fig. 3 identify the location and behavior of all 17 land cover classes. Now we can say MPGR-based classification is dependent upon dielectric constant or water content because water class is always have higher value in graph, and with greater values than ice, bare soil, and built-up areas. In terms of vegetation, dense or healthy vegetation is present near 0 and mixed, low, or degraded vegetation follows healthy vegetation (near 0.5). High values of PR-PR, PR-GR, and GR-GR indicate open water; the range of this value is larger because of the greater dynamic range in vegetation, soil, built-up, ice, and water. Although the use of the 89 GHz data requires a correction for atmospheric effects, it provides additional information to

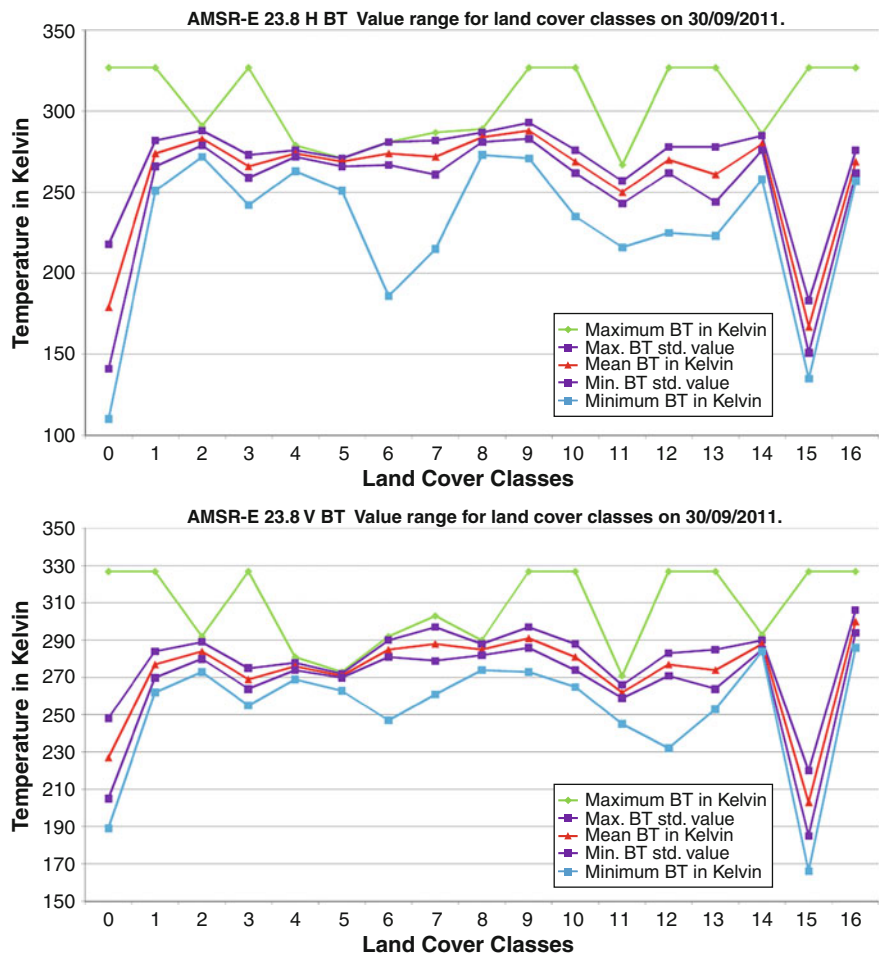


Fig. 2 continued

unambiguously distinguish weather effects from changes in land cover features. These results are similar with previous research results by Chen et al. [19] with land cover classification over China.

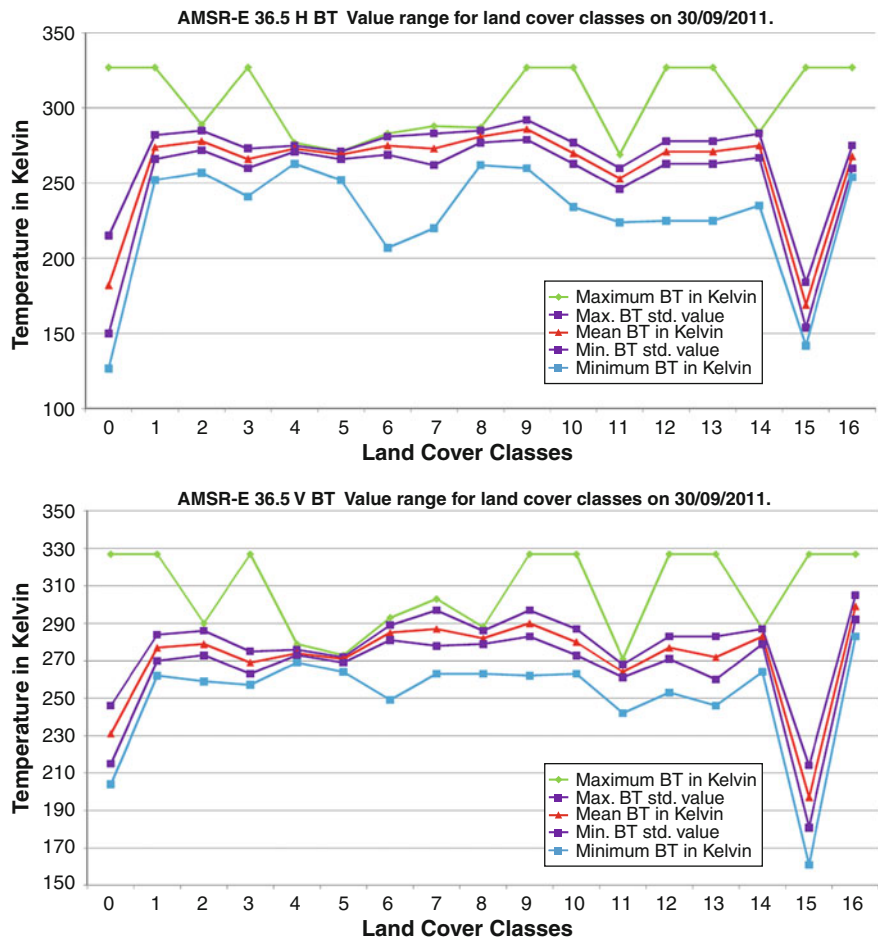


Fig. 2 continued

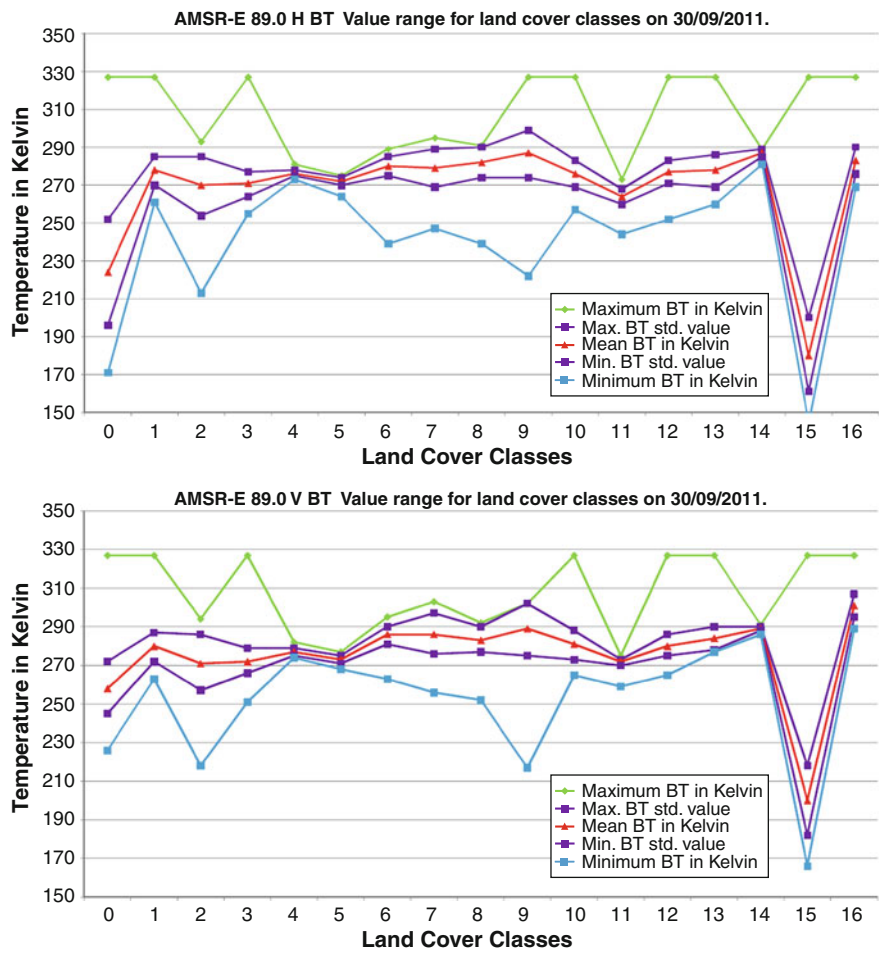
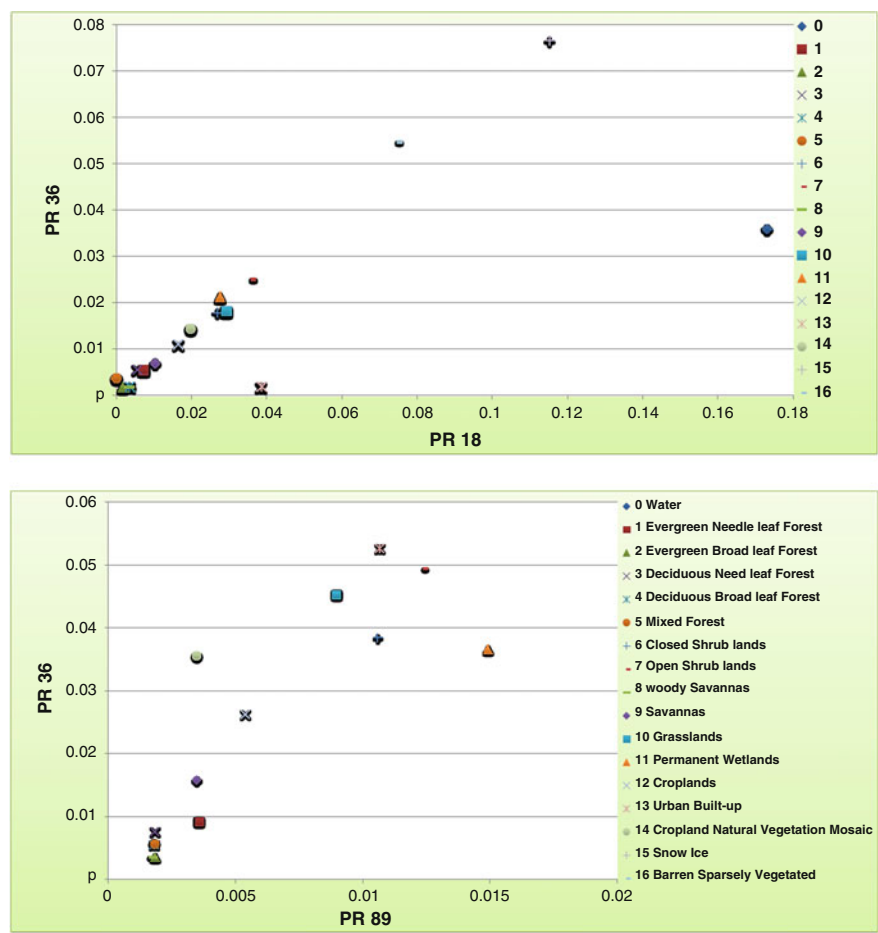


Fig. 2 continued



**Fig. 3** Seventeen land cover classes mean PR-PR (Fig A and B), PR-GR (Fig C and D) and GR-GR (Fig E and F) relation ratio with 10.7, 18.7, 36.5 and 89.0 Ghz H-V AMSR-E frequency

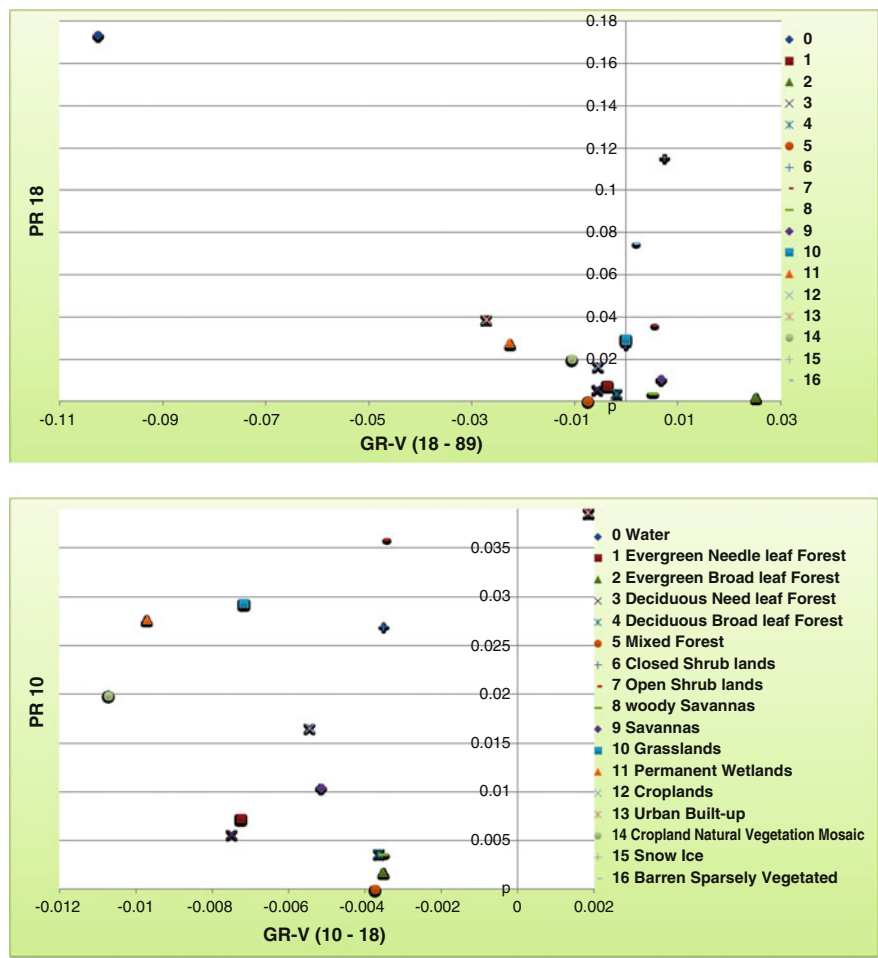


Fig. 3 continued

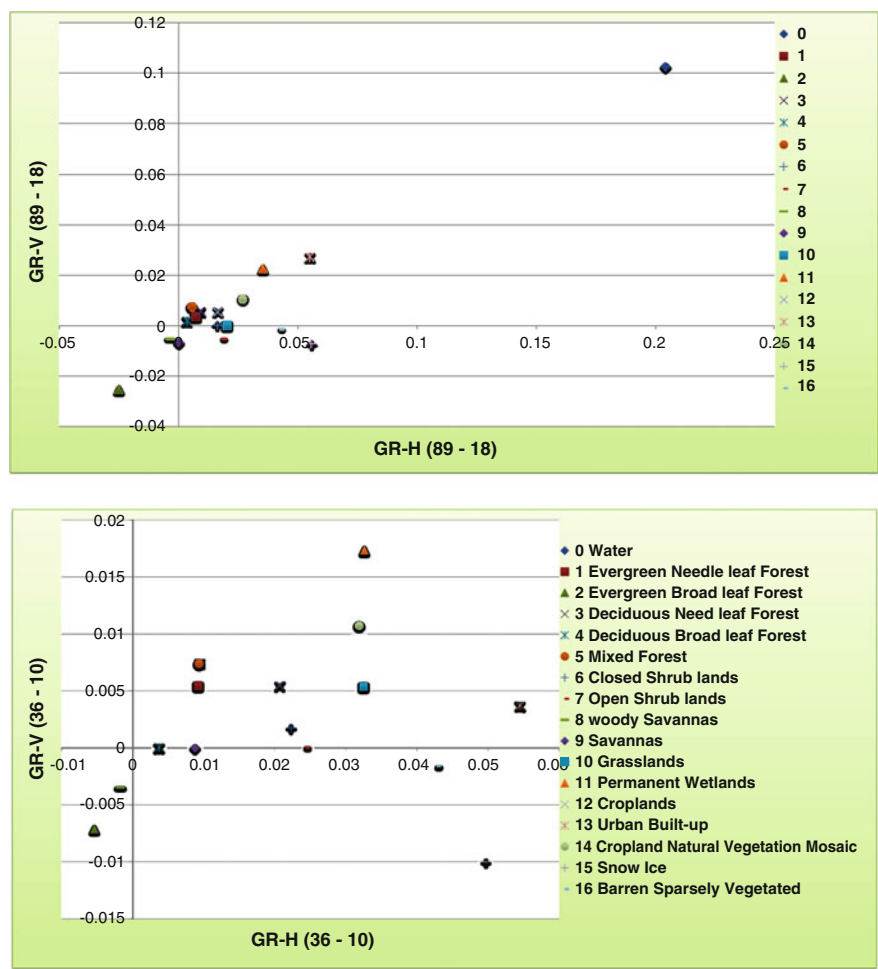


Fig. 3 continued



**Table 2** Land cover classes and there MPGR value

Land cover classes	PR-10	PR-18	PR-36	PR-89	GR-V (89-18)	GR-H (89-18)	GR-V (36-10)	GR-H (36-10)
Water	0.20-0.25	0.17-0.18	0.035-0.04	0.06-0.07	0.10-0.11	0.20-0.25	0.10-0.11	0.30-0.4
Evergreen Needle leaf Forest	0.005-0.01	0.005-0.01	0.005-0.01	0.00-0.005	0.00-0.005	0.005-0.01	0.005-0.01	0.005-0.01
Evergreen broad leaf forest	0.00-0.005	0.00-0.005	0.00-0.005	0.00-0.005	-0.02 to -0.03	-0.02 to -0.03	-0.01 to -0.005	-0.01 to -0.005
Deciduous needle leaf forest	0.005-0.01	0.005-0.01	0.005-0.01	0.00-0.005	0.005-0.01	0.005-0.01	0.005-0.01	0.005-0.01
Deciduous broad leaf forest	0.005-0.01	0.00-0.005	0.00-0.005	0.00-0.005	0.00-0.005	0.00-0.005	-0.005-0.0	0.00-0.005
Mixed forest	0.005-0.01	0.00-0.005	0.00-0.005	0.00-0.005	0.005-0.01	0.005-0.01	0.005-0.01	0.005-0.01
Closed shrub lands	0.035-0.04	0.025-0.03	0.015-0.02	0.01-0.015	-0.005-0.0	0.015-0.02	0.00-0.005	0.02-0.025
Open shrub lands	0.04-0.05	0.035-0.04	0.025-0.03	0.01-0.015	-0.01 to -0.005	0.015-0.02	-0.005-0.0	0.025-0.03
Woody savannas	0.00-0.005	0.00-0.005	0.00-0.005	0.00-0.005	-0.01 to -0.005	-0.005-0.0	-0.005-0.0	-0.005-0.0
Savannas	0.015-0.02	0.01-0.015	0.005-0.01	0.00-0.005	-0.01 to -0.005	0.00-0.005	-0.005-0.0	0.005-0.01
Grasslands	0.04-0.05	0.025-0.03	0.015-0.02	0.005-0.01	-0.005-0.0	0.02-0.025	0.005-0.01	0.03-0.035
Permanent wetlands	0.035-0.04	0.025-0.03	0.02-0.025	0.015-0.02	0.02-0.025	0.035-0.04	0.015-0.02	0.03-0.035
Croplands	0.025-0.03	0.015-0.02	0.01-0.015	0.005-0.01	0.005-0.01	0.015-0.02	0.005-0.01	0.02-0.025
Urban built-up	0.05-0.06	0.035-0.04	0.00-0.005	0.01-0.015	0.025-0.03	0.05-0.06	0.00-0.005	0.05-0.06
Cropland natural vegetation mosaic	0.03-0.035	0.02-0.025	0.01-0.015	0.00-0.005	0.01-0.015	0.025-0.03	0.01-0.015	0.03-0.035
Snow ice	0.13-0.14	0.11-0.12	0.07-0.08	0.05-0.06	-0.01 to -0.005	0.05 to -0.06	-0.02 to -0.01	0.05-0.06
Barren sparsely vegetated	0.09-0.10	0.07-0.08	0.05-0.06	0.035-0.04	-0.005-0.0	0.04-0.05	-0.005-0.0	0.04-0.05

**Table 3** MPGR based Land cover classification

MPGR range	PR-10	PR-18	PR-36	PR-89	GR-V (89–18)	GR-H (89–18)	GR-V (36–10)	GR-H (89–18)
-0.02 to -0.03					Evergreen broad leaf forest	Evergreen broad leaf forest		
-0.02 to -0.01							Snow ice	
-0.01 to -0.005					Savannas, snow ice, woody savannas, open shrub lands		Evergreen broad leaf forest	Evergreen broad leaf forest
-0.005 to -0.00					Barren sparsely vegetated/bare soil, bare soil, closed shrub lands, grasslands	Woody savannas	Woody savannas, barren sparsely vegetated/bare soil, deciduous broad leaf forest, savannas, open shrub lands	Woody savannas
0.00-0.005	Evergreen broad leaf forest, woody savannas	Mixed forest, evergreen broad leaf forest, woody savannas, deciduous broad leaf forest	Evergreen broad leaf forest, woody savannas, deciduous broad leaf forest, evergreen needle leaf forest, urban built-up, mixed forest	Evergreen broad leaf forest, woody savannas, deciduous broad leaf forest, mixed forest, evergreen needle leaf forest, savannas, cropland natural vegetation mosaic	deciduous broad leaf forest, evergreen needle leaf forest	Savannas, deciduous broad leaf forest	Closed shrub lands, urban built-up	Deciduous broad leaf forest
0.005-0.01	Deciduous broad leaf forest, mixed forest, deciduous need leaf forest, evergreen needle leaf forest	Deciduous need leaf forest, evergreen needle leaf forest	Evergreen needle leaf forest, deciduous need leaf forest, savannas	Croplands, grasslands	Deciduous need leaf forest, croplands, mixed forest	Mixed forest, evergreen needle leaf forest, deciduous need leaf forest	Evergreen needle leaf forest, croplands, grasslands, deciduous need leaf forest, mixed forest	Savannas, evergreen needle leaf forest, croplands, grasslands, deciduous need leaf forest, mixed forest
0.01-0.015		Savannas	Croplands, cropland natural vegetation mosaic	Closed shrub lands, open shrub lands, urban built-up	Cropland natural vegetation mosaic		Cropland natural vegetation mosaic	

(continued)

Table 3 (continued)

MPGR range	PR-10	PR-18	PR-36	PR-89	GR-V (89–18)	GR-H (89–18)	GR-V (36–10)	GR-H (89–18)
0.015–0.02	Savannas	Croplands	Closed shrub lands, grasslands	Permanent wetlands		Closed shrub lands, open shrub lands, croplands	Permanent wetlands	
0.02–0.025		Cropland natural vegetation mosaic	Permanent wetlands		Permanent wetlands	Grasslands		Croplands, closed shrub lands
0.025–0.03	Croplands	Closed shrub lands, grasslands, permanent wetlands	Open shrub lands		Urban built-up	Cropland natural vegetation mosaic		Open shrub lands
0.03–0.035	Cropland natural vegetation mosaic							Grasslands, cropland natural vegetation mosaic, permanent wetlands
0.035–0.04	Permanent wetlands, closed shrub lands	Open shrub lands, urban built-up	Water	Barren sparsely vegetated/bare soil		Permanent wetlands		
0.04–0.05	Grasslands, open shrub lands					Barren sparsely vegetated		Barren sparsely vegetated
0.05–0.06	Urban built-up		Barren sparsely vegetated	Snow ice		Snow ice, urban built-up		Snow ice, urban built-up
0.06–0.07				Water				
0.07–0.08		Barren sparsely vegetated	Snow ice					
0.08–0.09								

(continued)

Table 3 (continued)

MPGR range	PR-10	PR-18	PR-36	PR-89	GR-V (89-18)	GR-H (89-18)	GR-V (36-10)	GR-H (89-18)
0.09-0.10	Barren sparsely vegetated							
0.10-0.11								
0.11-0.12		Snow ice			Water		Water	
0.12-0.13								
0.13-0.14	Snow ice							
0.14-0.15								
0.15-0.16								
0.17-0.18		Water						
0.18-0.19								
0.19-0.20								
0.20-0.25	Water					Water		
0.25-0.30								
0.30-0.40								Water

## 5 Conclusion

This study is an attempt to use AMSR-E BT data for retrieving land cover classes. AMSR-E frequencies have relationship between land cover and MPGR values. Results confirm that the simplified land cover classification based on MPGR has the potential to reveal more precise land surface features from AMSR-E remote sensing data. Using a single day data, we classified the land surface into 17 types based on their MPGR values. Where all green/healthy vegetation comes near to 0.0 in polarization ratio and below then 0.0 in gradient ratio. Normal vegetation falls till 0.05 and then higher values for degraded or low vegetation/bare soil and built up. Highest values above 0.12 are for ice/water. This method can be used to target specific locations based on ground observations, but needs additional investigation, using data from different times of the year where the surface characteristics change. In addition, applying these relationships to independent data to learn about their stability also needs to be performed. Building an improved monitoring system for meteorological applications should be a subject of further research.

## References

1. Mao KB, Tang HJ, Zhang LX, Li MC, Guo Y, Zhao DZ (2008) A Method for retrieving soil moisture in Tibet region by utilizing microwave index from TRMM/TMI Data. *Int J Remote Sens* 29:2903–2923
2. Fily M, Royer A, Goitab K, Prigent C (2003) A simple retrieval method for land surface temperature and fraction of water surface determination from satellite microwave brightness temperatures in sub-arctic areas. *Remote Sens Environ* 85:328–338
3. McFarland MJ, Miller RL, Neale CMU (1990) Land surface temperature derived from the SSM/I passive microwave brightness temperatures. *IEEE Trans Geosci Remote Sens* 28 (5):839–845
4. Becker F, Choudhury BJ (1988) Relative sensitivity of normalized difference vegetation index (NDVI) and microwave polarization difference index (MPDI) for vegetation and desertification monitoring. *Remote Sens Environ* 24:297–311
5. Boori MS, Vozenilek V (2014) Assessing land cover change trajectories in Olomouc, Czech Republic. *Int J Environ Ecol Geol Min Eng* 8(8):540–546
6. Jackson TJ, Schmugge TJ (1991) Vegetation effects on the microwave emission of soils. *Remote Sens Environ* 36:203–212
7. Calvet JC, Wigneron JP, Mougin E, Kerr YH, Brito LS (1994) Plant water content and temperature of the Amazon forest from satellite microwave radiometry. *IEEE Trans Geosci Remote Sens* 32:397–408
8. Felde GW (1998) The effect of soil moisture on the 37 GHz microwave polarization difference index (MPDI). *Int J Remote Sens* 19:1055–1078
9. Owe M, Richard DEJ, Walker J (2001) A methodology for surface soil moisture and vegetation optical depth retrieval using the microwave polarization difference index. *IEEE Trans Geosci Remote Sens* 39:1643–1654
10. Choudhury BJ, Tucker CJ, Golus RE, Newcomb WW (1987) Monitoring vegetation using Nimbus-7 scanning multichannel microwave radiometer's data. *Int J Remote Sens* 8:533–538
11. Njoku EG, Chan SK (2006) Vegetation and surface roughness effects on AMSR-E land observations. *Remote Sens Environ* 100:190–199

12. Boori MS, Vozenilek V, Burian J (2014) Land-cover disturbances due to tourism in Czech Republic. *Advances in Intelligent Systems and Computing*, vol. 303. Springer, Switzerland, pp 63–72. doi:[10.1007/978-3-319-08156-4-7](https://doi.org/10.1007/978-3-319-08156-4-7)
13. Paloscia S, Pampaloni P (1988) Microwave polarization index for monitoring vegetation growth. *IEEE Trans Geosci Remote Sens* 26:617–621
14. Boori MS, Amaro VE (2011) A remote sensing approach for vulnerability and environmental change in Apodi valley region, Northeast Brazil. *Int J Environ Earth Sci Eng* 5(2):01–11
15. Boori MS, Amaro VE, Vital H (2010) Coastal ecological sensitivity and risk assessment: a case study of sea level change in Apodi River (Atlantic Ocean), Northeast Brazil. *Int J Environ Earth Sci Eng* 4(11):44–53
16. Clara SD, Jeffrey PW, Peter JS, Richard AM, Thomas RH (2009) An evaluation of AMSR-E derived soil moisture over Australia. *Remote Sens Environ* 113:703–710
17. Chris D (2008) The contribution of AMSR-E 18.7 and 10.7 GHz measurements to improved boreal forest snow water equivalent retrievals. *Remote Sens Environ* 112:2701–2710
18. Lubin D, Garrity C, Ramseier RO, Whritner RH (1997) Total sea ice concentration retrieval from the SSM/I 85.5 GHz channels during the Arctic summer. *Remote Sens Environ* 62:63–76
19. Boori MS, Amaro VE (2010) Land use change detection for environmental management: using multi-temporal, satellite data in Apodi Valley of northeastern Brazil. *Appl GIS Int J* 6 (2):1–15

Geoinformatics for Intelligent Transportation

Ivan, I.; Benenson, I.; Jiang, B.; Horák, J.; Haworth, J.;

Inspektor, T. (Eds.)

2015, XIX, 272 p. 111 illus., 86 illus. in color., Hardcover

ISBN: 978-3-319-11462-0